Pergamon

Journal of Structural Geology, Vol. 18, No. 4, pp. 505 to 517, 1996

0191-8141/96 $15.00+0.00

0191-8141(95)00082-8

The properties and geological environments of helicoids: axially symmetric surfaces in torsional and non-torsional deformations

T. J. FOWLER

Geology Department, La Trobe University Bendigo, P. O. Box 199, Bendigo, Victoria 3550, Australia

(*Received* 6 *February* 1995; *accepted in revised form* 14 *July* 1995)

Abstract—A helicoid is a non-developable surface swept out by a line (the generator) which rotates with constant sense about another, non-parallel line (the heliaxis) whilst moving parallel to that line in a constant direction. Torsion may produce helicoids, though this is not a necessity. Previous references to helicoids and helices in structural geology are reviewed, and the basic properties of helicoids are compared with those of cylindrical and conical surfaces. A map and stereogram technique is developed for the recognition of nested (initially parallel, equally rotated, coaxial) macroscopic helicoids. The typically sigmoidal outcropping traces of nested helicoids show dip-direction reversals along trend. On stereograms, linear loci, each representing the poles from a single helicoid trace, diverge from a common pole.

A nested set of macroscopic helocoidal cleavage surfaces from the Hill End Trough, southeastern Australia, are modelled and interpreted to have formed in two stages of torsion associated with accommodation of an adjacent granitoid intrusion. The volume affected by torsion is bound by curviplanar scissor faults.

Helicoids may be found associated with: rotational porphyroblasts, deformed cylindrical bodies or strip-like surfaces (e.g. intrafolial fold axial planes), cylindrical diapirs with helical flow patterns, cylindrical scissor-faults, ductile shear zones, zones of constrictional strain, and en échelon segmented dykes and fracture planes.

INTRODUCTION

Geometrical analysis of complexly deformed surfaces in structural geology has relied upon their reduction to approximate cylindrical segments (Weiss & McIntyre 1957, Turner & Weiss 1963), and occasionally conical segments (Stauffer 1964, Wilson 1967). Other ideal geometries have rarely been considered, an exception being the analysis of obliquely-folded surfaces by Ramsay (1967, Ch. 9). A helicoid is a surface produced when a line (the generator) is rotated, with constant sense, about another, non-parallel line (the heliaxis) whilst moving parallel to that line in one particular direction. Even in its most regular forms a helicoid is a non-cylindrical and non-conical surface. There have only been a few recent references in the geological literature to helicoids, probably due to the lack of definitions or methods of recognition of these surfaces.

This contribution aims first to clarify terms related to helicoidal surfaces, and also briefly considers terms associated with helical lineations. References to such geometries in the literature are then reviewed. The basic geometrical properties of helicoids are examined and compared with cylindrical and conical surfaces, with the intention of establishing criteria for the identification of helicoids from data on structural maps and stereograms. An example of a helicoidal cleavage trend surface from the southeastern Lachlan Fold Belt, Australia, is presented, and its probable origin discussed. Finally, the relationship between helicoidal geometries and torsional or other strains, and the nature of boundaries to domains containing helicoids (torsional and non-torsional) are discussed.

Terms associated with helicoids and helices

It is essential first to clarify the terms used in this paper for helicoids and helices (Table 1), since some of these terms have varied connotations between the science disciplines (i.e. mathematics, astronomy, geology and biology). Borowski and Borwein (1989) used the term 'helicoid' to refer to surfaces or solids with 'screw-thread

Table 1. Terms associated with helicoids and helices

Helix	A curved line produced when a point orbits a line (the heliaxis) while being translated parallel to that line in one particular direction. The helix is right-handed (Fig. 1a) if the point orbits the heliaxis clockwise, looking along the heliaxis. If the rotation is anticlockwise, a left-handed helix is produced (Fig. 1b).
Scrolled	Surfaces of cylindrical or conical geometry with a plane spiral section normal to their rotation axis. The scrolled surfaces shown in Fig. 1(c) are left-handed looking downwards onto these surfaces.
Helicoid	A non-developable surface produced when a line (the generator) is rotated about another, non-parallel line (the heliaxis) whilst moving parallel to that line in one particular direction. The helicoid is right-handed if the generator rotates clockwise around the heliaxis, looking along the heliaxis (Fig. 1d). If the rotation is anticlockwise, a left-handed helicoid is produced.
Spiral	If unqualified, this term is synonymous with 'helix'. A *plane spiral* or *planospiral* is a plane curve generated by a point which orbits another point in that plane, while consistently approaching or receding from it. The planospirals shown in Fig. 1(e) are left-handed, looking onto the plane.

appearance'. This is too informal for practical use. James and James (1992) more precisely define a helicoid as a surface 'generated by a plane curve or twisted curve which is rotated about a fixed line as axis, and is also translated in the direction of the axis in such a way that the ratio of the two rates is constant'. This definition has been modified for the purposes of this paper (Table 1) by specifying a constant direction of translation and constant sense of rotation, and non-parallelism of generator and axis, but removing the requirement for a constant ratio of rates of translation and rotation. Also, the generator of the helicoid surface is simply referred to as a 'line', which places no limitations on the shape of that line. Similarly the axis of rotation (here referred to as the heliaxis) may also be rectilinear or curvilinear (plane or non-plane).

The terms 'helicoidal' and 'helical' are regarded in biological literature as being synonymous, and have also been used in this sense by Ramsay (1967, p. 493) and Hippertt (1994). To avoid confusion, it is recommended that 'helical' be used in preference to 'helicoidal' when referring to a helix. The term 'spiral' has been used to describe: (i) plane curves formed by a point orbitting another point whilst (consistently) approaching or receding from the latter (e.g. spiral inclusion patterns in syn-kinematic rotational porphyroblasts), and (ii) helices. It is recommended that when sense (i) is intended the term 'plane spiral' or 'planospiral' be used (Table 1). While the term 'twisted' seems convenient to use in connection with torsion, the term has been avoided in this paper since it has a separate definition in mathematics where it refers to non-plane lines (see definition of 'helicoid' by James & James (1992) above).

Some surfaces have plane spiral sections but have cylindrical or conical geometry in three-dimensions (Fig. 1c). A separate term 'scrolled' (Table 1) is used to describe such surfaces. It is recommended that imprecise terms like 'coiled' or 'convolute' should not be used, at least in reference to statistical geometrical analyses.

A helix may be described as right- or left-handed. It is right-handed if the point tracing out the helix appears to have moved clockwise as it moves away from an observer looking along the heliaxis (Fig. 1a). It is left-handed if this sense of rotation is anticlockwise (Fig. 1b). In a similar manner, a helicoid (Fig. 1d) is right-handed if the surface appears to be generated by a line which rotates clockwise as the line moves away from an observer looking along the heliaxis. As shown in Figs. 1(a, b & d), the right- or left-handedness is independent of the direction of observation along the heliaxis. Planospirals and scrolled surfaces are also right- or left-handed; however, a direction of observation must be nominated. Both examples of scrolled surfaces in Fig. 1(c), and the planospirals in Fig. 1(e) are left-handed as a result of the anticlockwise sense of propagation of the surfaces (or lines) away from their orbiting axes (or point), with the observations being made from the top of the figure downwards for Fig. 1(c), and looking onto the plane in Fig. 1(e).

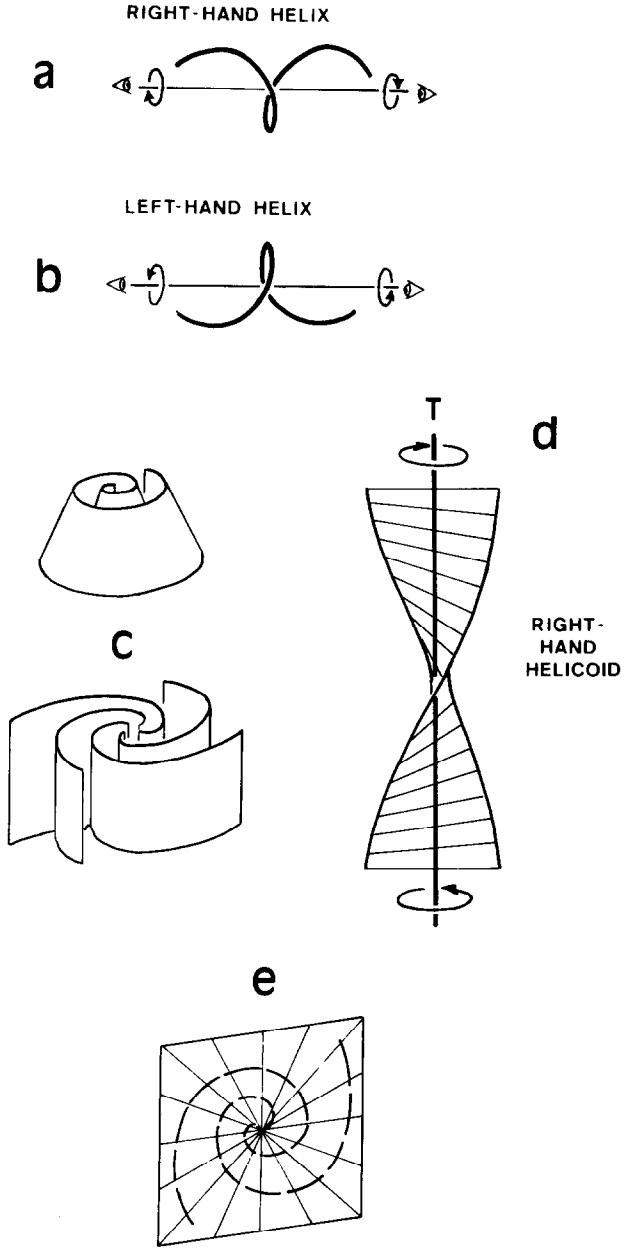

Fig. 1. (a) A right-hand helix is produced by a point which orbits an axis clockwise as it moves parallel to the axis away from the observer. (b) A left-hand helix is produced by a point which orbits an axis anticlockwise as it moves parallel to the axis away from the observer. (c) Scrolled surfaces with conical and cylindrical geometry. Both are left-handed looking downwards at these surfaces. (d) A right-hand helicoid is produced by a line which rotates about an axis clockwise as it is translated parallel to the axis, away from the observer. (e) A plane spiral (planospiral) is a plane curve generated by a point which orbits another point in the plane, while consistently approaching or receding from it. Looking onto the sketched plane, a coplanar pair of left-hand planospirals may be seen. (Further definitions in Table 1.)

References to helicoids and helices in the geological literature

There have been a few references in the geological literature to terms associated with helical and helicoid geometry. These references include the following.

1. The complex internal foliations defined by inclusions within syn-tectonic rotated porphyroblasts are commonly referred to as spiral inclusion trails (Powell &

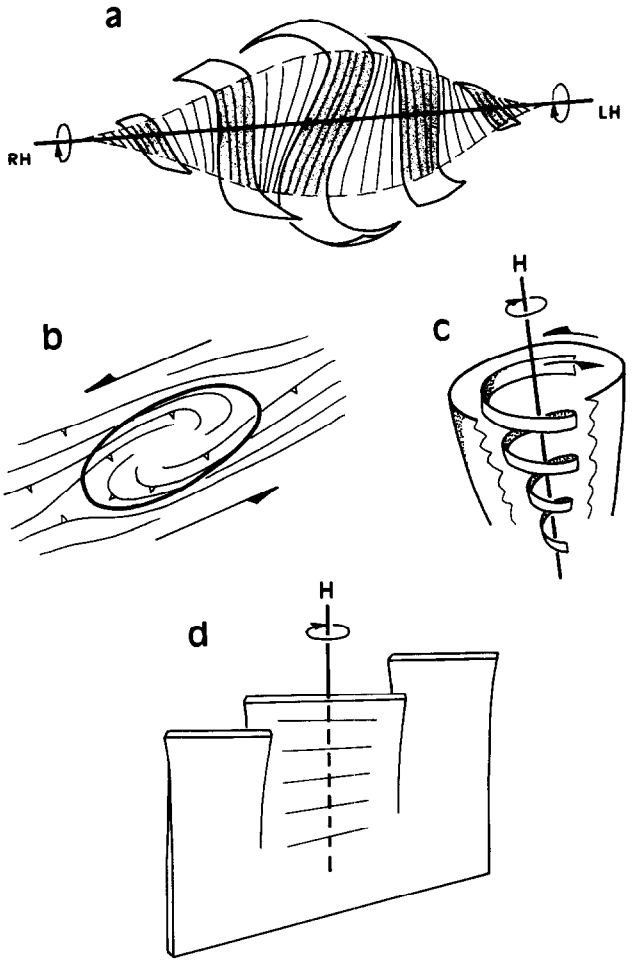

Fig. 2. Examples of geological scrolls, helices and helicoids. (a) Slices through a rotational porphyroblast, showing the internal foliation. The shaded portions of the surface form two helicoids (one right-hand (R), the other left-hand (L)). (b) Apparently scrolled foliations within a ballooning pluton intruded into an active shear zone (after Brun & Pons 1981). (c) Helical magmatic flow in a diapir (after Hippertt 1994). (d) Right-hand helicoid-shaped dyke segments in the transition from single planar dyke to en échelon dyke system (after Fink 1985). In (a), (c) and (d) H represents the heliaxis.

Treagus 1967, 1970, Rosenfeld 1970, Schoneveld 1977). These porphyroblasts show plane spiral sections normal to the rotation axis. The internal foliation surface is a scrolled helicoid, that is scrolled in slices through the centre, normal to the rotation axis and helicoidal in a core, coaxial with the rotation axis (Fig. 2a). Powell and Treagus (1967, 1970) and more recently Johnson (1993) illustrated the helicoid surface geometry along the rotation axis via serial sections through garnet porphyroblasts.

2. Watkinson (1981, fig. 5) illustrated an apparently 'twisted' mesoscopic fold axial plane. He noted that isolated fold shapes such as intrafolial folds may sustain a twisting (torsional) mode of buckling.

3. Helical flow in diapirs (Fig. 2c), with the consequent development of helical flow fabrics, has been described by Hippertt (1994). Hippert (1994) described left-handed helical lineations related to rotation during diapiric rise. These lineations lay on conically-nested foliations outlining flow cells. He also suggested that those internal structures shown by Bouchez *et al.* (1990) might also be helical, and that the helical pattern may relate to slow diapiric ascent. Brun and Pons (1981) examined the Salvatierra pluton, which they described as having been emplaced as an expanding diapir in an active transcurrent shear zone. The pattern of foliations within the Salvatierra pluton were described as 'helicoidal' due to interference between ballooning and transcurrent shear. The foliation trend surfaces describe plane spirals on their map, but the steep dip of the foliations suggests either a cylindrical or conical scrolled geometry (e.g. Fig. 2b).

4. En échelon dykes, which form by break-up during ascent of a single steeply-dipping dyke into segments, each of which rotates through roughly the same angle and in the same sense (Anderson 1951, Delaney & Pollard 1981, Fink 1985), are helicoidal in shape (Fig. 2d). Mandl (1987, p.109) illustrated segmentation of propagating fracture planes in three-dimensional stress fields into a series of helicoidal finlike surface components, which formed in stress fields where the orientation of the principal stress, σ_3, rotated progressively with depth.

5. Global scale spiral lineaments have been noted by O'Driscoll (1980), who discovered a fundamental left-handed double helix lineament pattern emanating from the Earth's poles and wrapping obliquely around the Earth. A counterspiral trend (right-handed) was also identified. These were perceived to have exerted a control on continental outlines and locations of major tectonic elements (island arcs, fold belt systems).

BASIC GEOMETRICAL PROPERTIES OF HELICOIDS

Whereas complete mesoscopic examples of helicoids may be relatively simple to recognise (e.g. Watkinson 1981, fig. 5), identification of a macroscopic helicoid (e.g. by sampling poles on isolated parts of the surface) requires statistical analysis. To this end it is necessary to investigate the basic geometrical properties of helicoids. Of the infinite variety of helicoids, only the most regular helicoids will be treated here, namely those with rectilinear generators and heliaxis, and constant rate of translation relative to rotation. Non-regular helicoids are discussed briefly later.

Cylindrical, conical and simple helicoid surface segments are compared in Fig. 3. The cylindrical surface can be pictured as being generated by a line (a fold axis) which is parallel to the rotation axis (Fig. 3a). The cone is generated by a line inclined to and rotating about the cone axis (Fig. 3c). For cylindrical and conical surfaces, the poles to the surface have constant orientation along any of the lines which trace out their surface. Therefore, on a stereogram these surfaces are represented by one point per generating line, allowing the surfaces to be represented by a single curvilinear locus of points—a great or small circle curve, respectively (Figs. 3b&d). In addition, the generators of conical and cylindrical surfaces intersect each other if extended far enough in

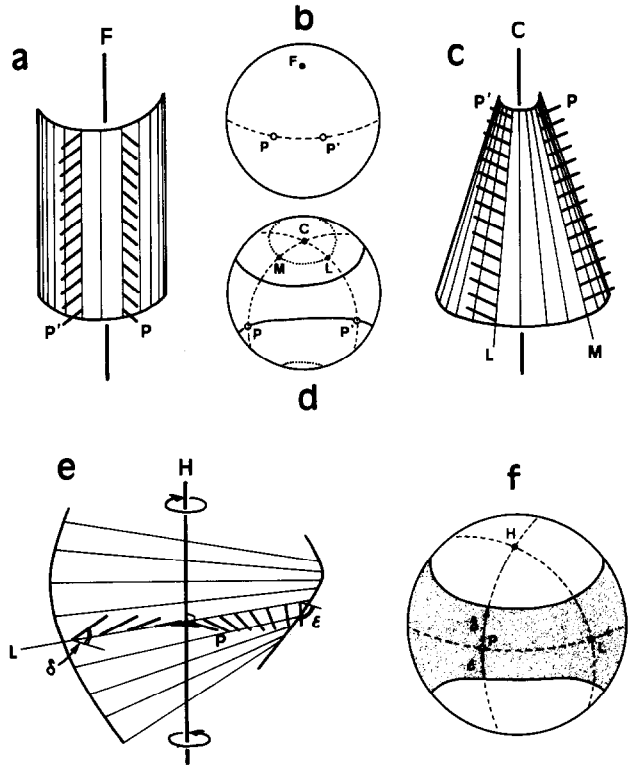

Fig. 3. Comparison of the geometry of cylindrical, conical and helicoid surfaces. (a) Cylindrical surface with cylinder axis F. Along each line tracing out the cylinder surface, poles (e.g. P, P') have constant orientation. (b) Stereographic representation of geometry in (a). P & P' lie on a great circle, with F as its pole. (c) Conical surface with cone axis C. Along each line tracing out the cone surface (e.g. M & L), poles (P & P', respectively) have constant orientation. (d) Stereographic representation of geometry in (c). P & P' lie on a small circle, with C as cone axis. L & M lie on another small circle coaxial with C. C, M & P lie on a great circle, as do C, L & P'. (e) Right-hand helicoid surface with heliaxis H. Poles along each line (e.g. L), tracing out the surface vary so that they are normal to H (pole P) at the heliaxis, but rotate towards parallelism with H as radial distance from H increases. Therefore for each line like L, there is a population of poles, and the helicoid is represented by an area of poles on the stereogram. (f) Stereographic representation of helicoid surface in (e). Poles scatter away from the great circle (through P & L), which has H as its pole. The area of poles on the stereogram is bound by two small circles, coaxial with H. The small circle cone angles are determined by the radial distance from H over which poles to the surface are collected (in this case at distances such that the poles at the margins of the helicoid subtend angles δ and ε, respectively, with P, as shown).

space. Surfaces with generators showing these properties are referred to as developable surfaces (Lisle 1992). For the helicoid (Fig. 3e), the poles along each generator change their orientation as follows. At infinite radial distance these poles are parallel to the heliaxis. Moving radially towards the heliaxis these poles rotate so that the pole at the heliaxis is normal to this axis (Fig. 3e). Each generator line has a population of poles, and therefore poles to a helicoid segment are dispersed over an area of the stereogram. The regular helicoids described here are ruled surfaces; however, they are non-developable since the generators do not intersect with each other.

If the generator of the helicoid touches the heliaxis, the poles collected along the heliaxis plot on a stereogram on the great circle normal to it. Poles collected at radially-greater distances from the heliaxis scatter further away from this great circle (Fig. 3f). Where the helicoid generator is skew to the heliaxis, the poles scatter away from a small circle, with cone axis parallel to the heliaxis. In the latter case, poles on the generators at their points of closest approach to the heliaxis lie along this small circle. These points of closest approach themselves trace out a helix. On the stereogram, the angular radius of the small circle of poles depends on the ratio of the rate of translation to the rate of rotation of the helicoid generator, and the diameter of the helix of closest points.

The obliquely-folded surfaces described by Ramsay (1967, Ch. 9) superficially resemble helicoids, but are more closely related to cylinders and cones. After oblique folding, any set of initially parallel surfaces is represented on a stereogram by a single curvilinear line of points varying (depending on the original orientation of the oblique plane with respect to the fold axis) between a great and a small circle.

Ideally, the above properties could be used to distinguish helicoid segments from cylindrical or conical segments, and the heliaxis could be located. In practice the above properties are unlikely to be sufficient to identify macroscopic helicoids for the following reasons. When initially planar parallel surfaces (e.g. beds) are cylindrically- or conically-folded on the macroscale, it is usual practice to combine orientation data on a stereogram obtained from all of the folded surfaces around a single fold, because the poles from each folded surface describe the same pattern on the stereogram. This is not the case for members of a set of nested helicoid surfaces, because each member of the set has a different representation of poles on a stereogram. This is because each member is formed by a generator increasingly distant from the heliaxis. Since it is unlikely to be able to sample the poles from a continuously-exposed macroscopic helicoid surface, it is necessary to include map characteristics in the identification of these surfaces. A similar approach was taken by Hippertt (1994) to discriminate between conically-arranged and helical lineations, which cannot be distinguished by stereographic analysis alone. An additional problem with relying solely on the stereographic properties of helicoids for their recognition, is that surfaces represented by poles which scatter away from a great or small circle on a stereogram are generally regarded as approximately cylindrical or conical. This may partially explain why helicoids have been overlooked in structural analysis.

For macroscopic nested helicoids, two approaches to their recognition from surface structural maps are described below. These examine: (i) the shapes of curvilinear outcrops of a set of nested helicoid surfaces exposed on a horizontal erosion surface (these curves are referred to as helicoid traces), and (ii) the helicoid surface dips along the helicoid traces, represented as poles on a stereogram. The locus of poles on a stereogram representing data collected from a single helicoid trace is referred to here as a pole locus (plural — pole loci). The identification criteria which are described below were developed by mathematically modelling

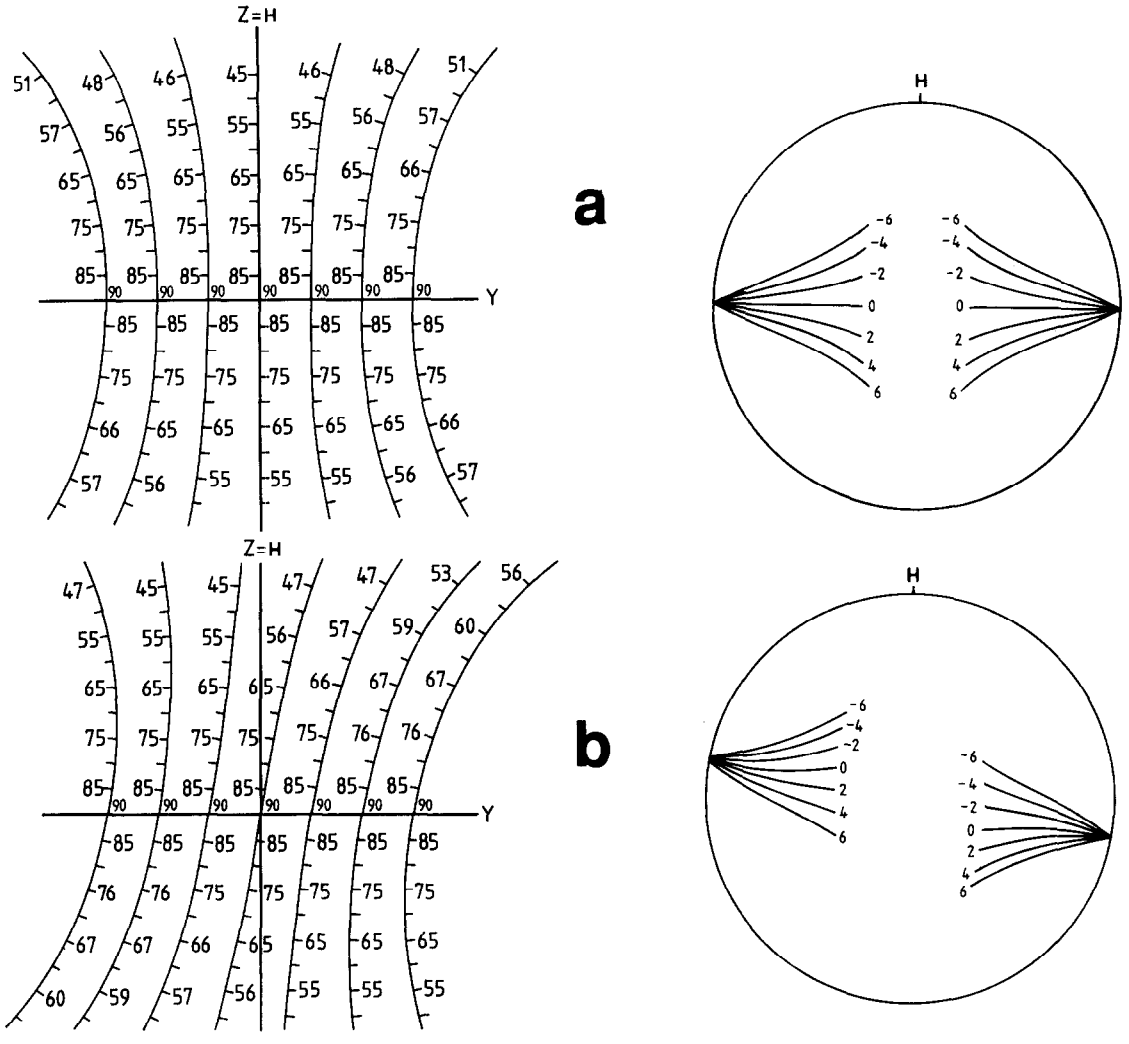

Fig. 4. Helicoid traces formed by intersection of horizontal erosion surface with nested helicoids, originally a set of vertical planar parallel surfaces striking N–S, parallel to z, spaced at two-unit intervals along y, and subsequently rotated +5° per unit distance along $H = z$. Dips of the outcropping helicoids are shown. Stereographic representation of pole loci (a line of poles collected along the outcropping trace of a single helicoid) are also shown, and numbered according to the y intercepts for the original planes. Note the two-fold symmetry axis along x (vertical reference axis emerging from intersection of y and z axes). (a) H crops out along the surface. (b) H lies at depth $x = 2$. See text for further discussion of these patterns.

helicoids formed from initially planar surfaces (see Appendix), and exploring patterns produced by widely-varying orientation and geometrical parameters.

PROPERTIES OF HELICOID TRACES ON STRUCTURAL MAPS

Two simple situations are considered: (a) the heliaxis is parallel to the erosion surface (and lies on, above or below it), and (b) the heliaxis plunges, therefore emerging at some point on the map surface. In either case the original planar surfaces may be parallel or oblique to the heliaxis. In all of the following figures and discussion, the Cartesian reference axes used to describe the helicoid traces and surfaces are z (N–S and horizontal, with $+z$ pointing N), y (E–W and horizontal) and x (vertical). The horizontal erosion surface therefore corresponds to a plane with constant x values. For the situation where the heliaxis is horizontal, the z-axis is set along it.

Considering first a buried horizontal heliaxis, Fig. 4 shows two examples of patterns of helicoid traces and associated stereograms for poles collected along these traces. For both examples in Fig. 4, the original orientation of planes was N–S vertical, i.e. parallel to the heliaxis (i.e. the z-axis). The planes have been subject to +5° (i.e. right-handed) rotation per unit distance along z. Figure 4(a) has z lying on the erosion surface (i.e. the erosion surface is the plane $x = 0$), while in Fig. 4(b) z is buried at depth ($x = 2$). In Fig. 4, helicoid traces and pole loci show a vertical 2-fold symmetry axis, corresponding to the x-axis. This is true for any section parallel to z, when z lies parallel to the original planar surfaces, because such helicoids belong to the $D\infty$ point group (Paterson & Weiss 1961), with ∞ 2-fold axes winding normal to z. Helicoid traces diverge away from the y axis and have opposite senses of curvature on either side of the origin. Each curve shows dip direction reversals along trend, with the locations of vertical dips lying along the y-axis. The curve through the origin is straight in Fig. 4(a), but sigmoidal in (b). In Fig. 4(b) the sigmoidal curve above the origin is s-shaped (for right-handed rotation) if the z axis is below the surface, and z-

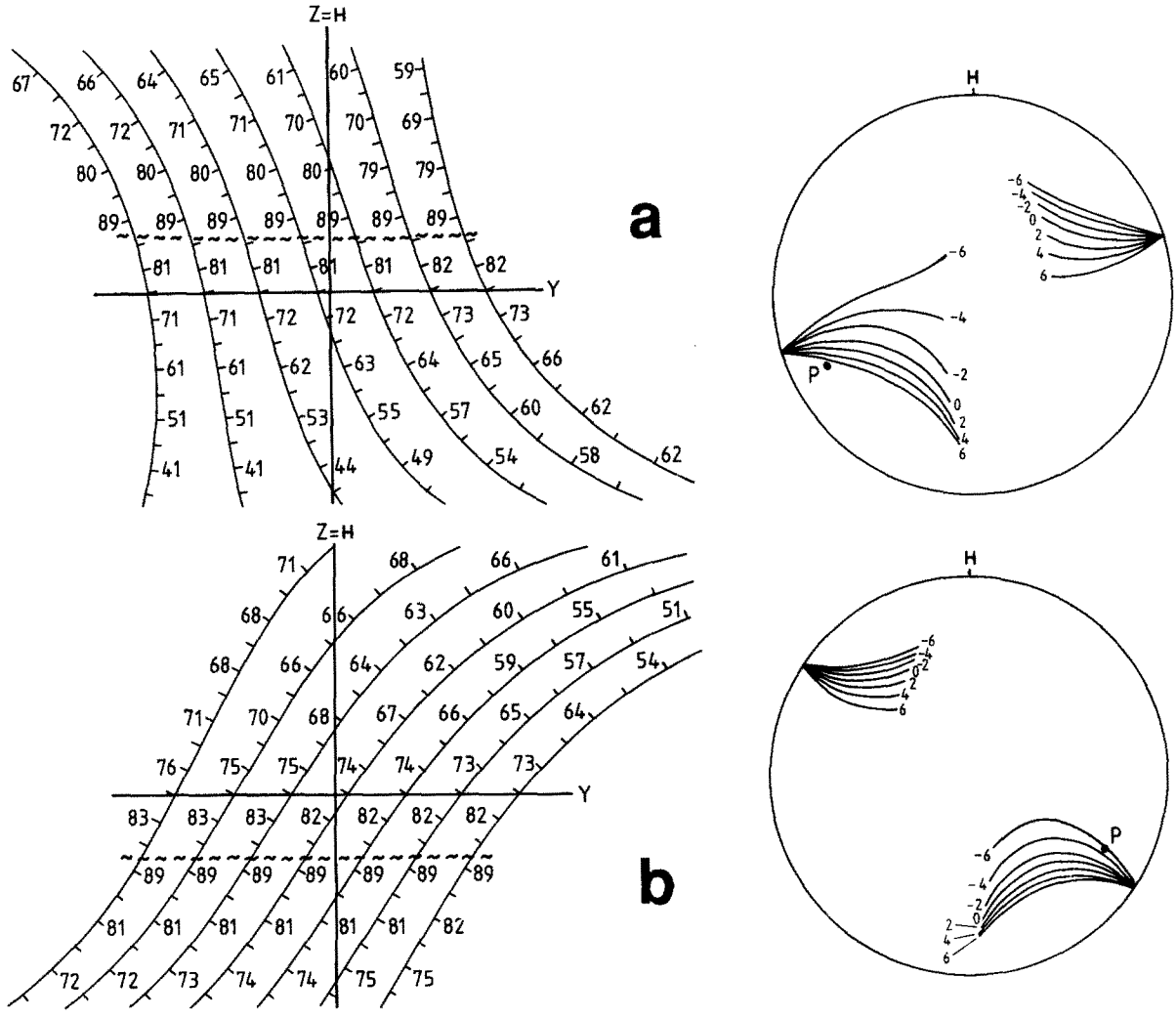

Fig. 5. Helicoid traces and stereogram pole loci as for Fig. 4(b) (i.e. heliaxis at depth $x = 2$), except that the original orientation of planes before rotation was oblique to H, being N27W 77NE in (a), and N27E 77NW in (b). The pole to the original planes is represented by the point P on the stereogram in both (a) and (b). The broken line cutting across the helicoid traces represents the locus of points of dip reversal. See text for discussion of these patterns.

shaped if it is above. The opposite relations are true for left-handed rotation. There is thus ambiguity regarding locating a horizontal heliaxis from its helicoid trace patterns. For both Figs. 4(a)&(b) (and for all cases where the heliaxis is horizontal), the pole loci diverge from a single common horizontal pole which is normal to z at $x = 0$, but approaches z at higher values of x. Pole loci curve strongly to approach z at large z values. The points on the helicoid traces corresponding to the common pole all lie along the y-axis, that is are coincident with the locus of points of dip-direction reversal.

Helicoid traces and pole loci are shown in Fig. 5 for a buried horizontal heliaxis, with initially oblique planar surfaces. For both Figs. 5(a)&(b), rotation is +5°, and z lies at depth $x = 2$, but in (a) the original surfaces had orientation N27W 77NE, while in (b) they were N27E 77NW. Here both helicoid traces and pole loci lack symmetry because they belong to the $C\infty$ point group (Paterson & Weiss 1961), which lacks 2-fold axes of symmetry. Sigmoidal helicoid traces are common, and reversals of dip along trend are again the rule, but the points of dip reversal do not generally coincide with curvature maxima or curve inflections. Nevertheless, these dip reversal locations lie on a line parallel with the y-axis (i.e. normal to the heliaxis). Helicoid traces again diverge away from the y-axis. All pole loci for these two families diverge from a common horizontal pole to approach the z axis. Again the points on the helicoid traces corresponding to the common pole are coincident with the locus of points of dip-direction reversal. As noted above, there is ambiguity regarding whether the heliaxis lies above or below the surface, unless the sense of rotation (right- or left-handed) is known.

The most general condition for regular helicoids is for a plunging heliaxis and initially oblique initially planar surfaces. Two examples are shown in Fig. 6. In both Figs. 6(a)&(b), the original surfaces were N27W 77NE, and deformation involved +5° rotation per unit length along the heliaxis. The heliaxis plunges 10 and 30° north, respectively for Figs. 6(a) & (b), and emerges at the origin of the reference axes. For this situation, the heliaxis no longer lies along the z-axis. The z-axis is horizontal and lies N–S along the erosion surface, which is represented by the plane $x = 0$. A gently plunging

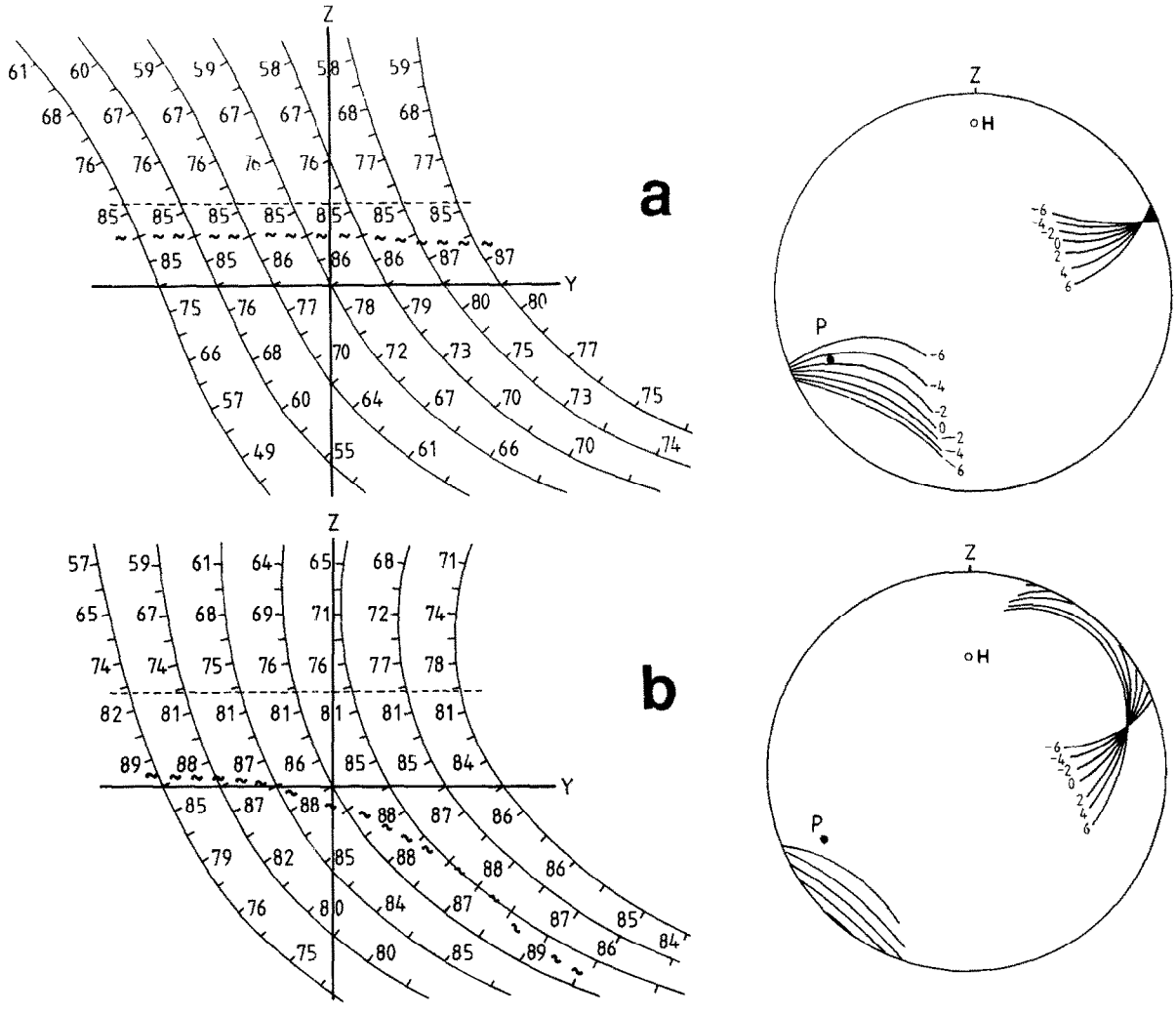

Fig. 6. Helicoid traces and pole loci for two situations where the heliaxis plunges towards the N from the origin. z is horizontal and lies on the erosion surface which is represented by the plane $x = 0$. The orientation of planes before rotation was N27°W 77NE (with pole to these planes represented by P on the stereograms). Plunge of H is 10°N in (a) and 30°N in (b). H is also represented on the stereograms. The wavy broken line cutting across the helicoid traces represents the locus of points of dip reversal, while the dashed line normal to z represents the locus of points corresponding to the common pole on the stereogram. See text for discussion of these patterns.

heliaxis yields sigmoidal helicoid traces (Fig. 6a). As the plunge of the heliaxis increases the helicoid traces adopt the same curvature sense (Fig. 6b), though still show reversals of dip direction along trend. Notice that in Fig. 6(b) the locus of points of dip reversal does not approximately parallel the y-axis. Pole loci again intersect in a common pole which is now not horizontal. With increasing plunge of the heliaxis the common pole becomes steeper, and the pole loci condense and become a single great circle when the heliaxis is vertical. The points on the helicoid traces corresponding to the common pole still lie on a straight-line locus which is perpendicular to the trend of the heliaxis, though here is distinct from the locus of points of dip-direction reversal.

Summary of the properties of helicoid traces—criteria for recognition of helicoids

Helicoid traces are characterised by changes in dip sense along trend, with the points of dip reversal lying on a line lying typically at a large angle to the overall trend of the helicoid traces. In general, the locations of dip reversals are independent of curvature maxima or inflections of the helicoid traces. A propellor-blade geometry for the individual surfaces is usually evident, though the helicoid traces need not be sigmoidal. Because of the axial symmetry of helicoids, these patterns would be conserved if the entire set of helicoids were tilted (without changing the plunge of the heliaxis). The effect of tilting would be to translate the patterns parallel to the z-axis.

Although obliquely-folded surfaces may also show dip reversals and sigmoidal traces in section, these surfaces may be distinguished from helicoids by their pole loci on a stereogram, as explained previously. Distinguishing a single obliquely-folded surface from a single helicoid will, however, require more data than mere poles to curvilinear lines of intersection.

Pole loci plotted for sets of helicoid traces intersect in a common pole which is horizontal if the heliaxis is horizontal, and plunges if the heliaxis plunges. These pole loci diverge away from the common pole. The pole

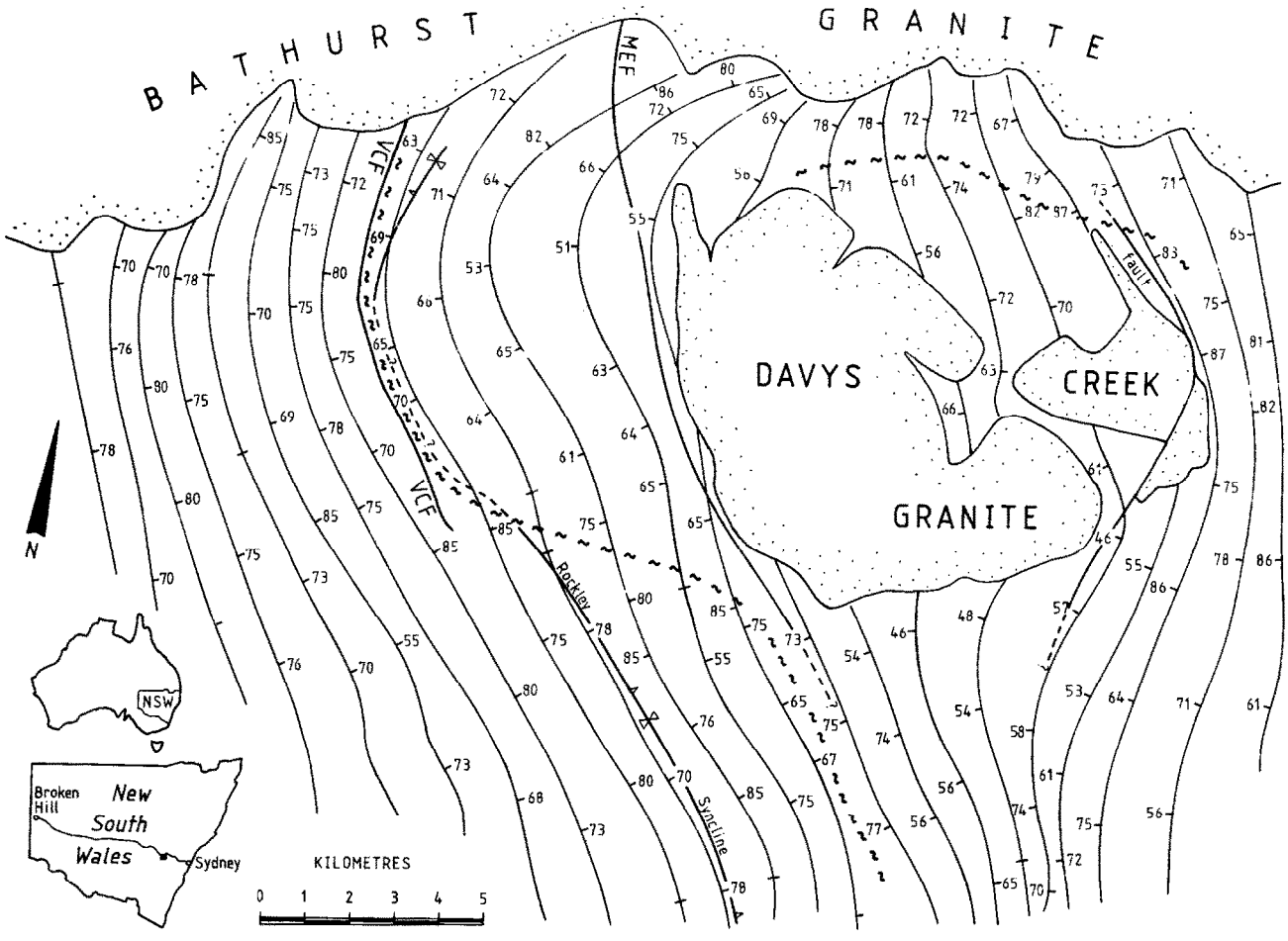

Fig. 7. Map of the cleavage trend surfaces and cleavage dips in the Rockley district, Hill End Trough, southeastern Australia. The sigmoidal propellor-blade shaped axial plane of the Rockley Syncline is shown. The broken lines cutting across the cleavage trends represents the locus of points of local cleavage dip reversal. VCF = Vale Creek Fault. MEF = Mt Evernden Fault. See text for discussion and interpretation of the patterns.

loci will show a 2-fold symmetry only if the original surfaces contained the heliaxis. The set of points on the helicoid traces corresponding to the common pole lie on a line perpendicular to the trend of the heliaxis. Since the common pole represents identically-oriented tangents to the nested helicoid surfaces, the mapped line of points corresponding to it is also an isotrend line as described by Lisle (1992).

The above criteria should be sufficient to identify approximately regular macroscopic helicoid surfaces and to gain an idea of the orientation of the heliaxis. However, trial-and-error modelling is likely to be necessary to locate the heliaxis geographically and to determine amount of rotation per unit distance along it.

HELICOIDAL CLEAVAGE TREND SURFACES FROM THE LACHLAN FOLD BELT, SE AUSTRALIA

A mapped portion of the deformed Palaeozoic Hill End Trough in the Lachlan Fold Belt, southeastern Australia, is presented in Fig. 7. The thick marine sequence of sediments and volcanics of the Hill End Trough were deformed by roughly E–W compression in the mid-Carboniferous Kanimblan Orogeny (Powell 1984). This deformation generated macroscopic folds and an associated penetrative steeply-dipping slaty cleavage. In the northern part of the trough, north of the Bathurst Granite, the cleavages describe a convergent cleavage fan with almost rectilinear cleavage trend lines extending roughly north–south. Also in this part of the trough, the line dividing easterly-dipping cleavages from westerly-dipping cleavages is not oblique to the cleavage trends (Collins 1971). South of the Bathurst Granite (Fig. 7), the cleavages also define a macroscopic fan, though cleavage trends are moderately to strongly curved, are sometimes sigmoidal, and have dip reversals along trend giving the cleavage trend surfaces a propellor-blade geometry. The locus of points of dip reversal lies at a large angle to the cleavage trends. The main macroscopic fold structure, the Rockley Syncline, has an axial plane which is gently sigmoidal and has a propellor-blade geometry (Stanton 1956, Fowler 1989).

The eastern part of the cleavage fan shown in Fig. 7 has been intruded by the late syntectonic Davys Creek Granite (Fowler 1994). There are two reverse faults (the Vale Creek Fault and the Mt Evernden Fault) which extend at least as far south as the southern edge of the Davys Creek Granite. The Vale Creek Fault is a curved

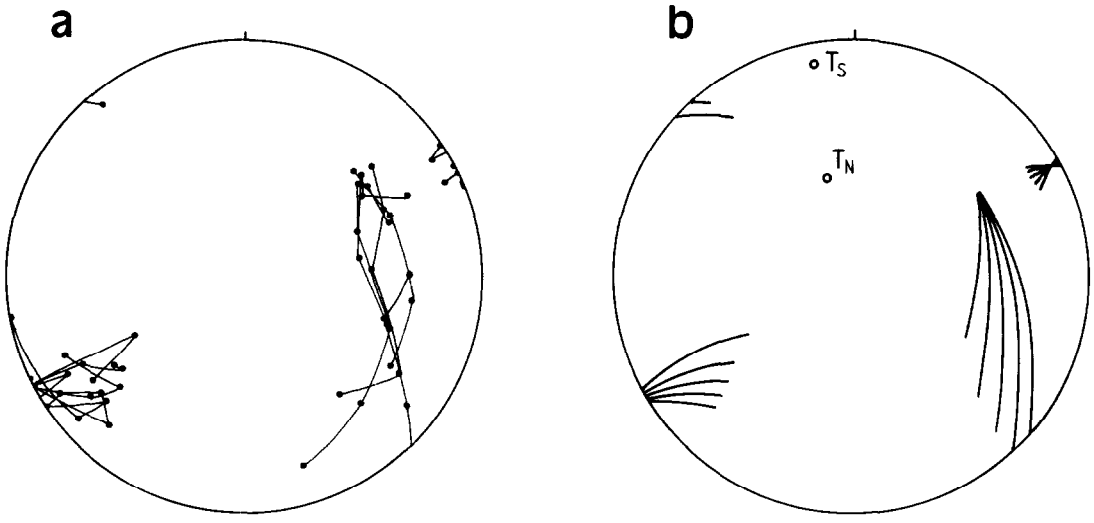

Fig. 8. (a) Pole loci for the cleavage trend surfaces in the Rockley district cleavage fan between the Vale Creek and Mt Evernden Faults, shown in Fig. 7. (b) Best-fit helicoid pole loci corresponding to (a). T_s and T_N are estimated heliaxes for the southern and northern halves of this helicoidal domain, respectively.

scissor fault with increased displacement at its northern end (Fowler 1987).

The poles measured along cleavage trends plot as two sets of diverging pole loci on a stereogram, each with a common pole (Fig. 8). On the basis of the above properties it is proposed that the cleavage trend surfaces in the southern part of the Hill End Trough have helicoidal geometry. The following presents results of trial-and-error mathematical modelling of the helicoidal surfaces to locate the heliaxis and estimate the amount and sense of rotation involved.

Torsional origin of the helicoidal cleavage trend surfaces in the southern Hill End Trough

The stereographic plot of poles measured along the outcropping cleavage trend surfaces for the southern part of the Hill End Trough is presented in Fig. 8(a). The best fit for both mapped helicoid traces and pole loci is shown for comparison in Figs. 8(b) and 9. It is clear that there has been some complexity in the history of deformation of these cleavages. The model of best fit requires that the heliaxis changes plunge from 5° (towards N10W) south of the southern edge of the Davys Creek Granite to 46° (towards N15W), in the region west of the Davys Creek Granite bound by the Vale Creek and Mt Evernden Faults. The orientation of the original planar surfaces in the southern part was estimated to be N30W vertical, while in the northern part they were approximately N40W 78SW. The two sets of pole loci correspond with these two apparently different helicoidal sections of the cleavage trend surfaces. As far as can be determined by trial-and-error of a large range of values, there are no significantly different solutions which satisfy the data.

The interpreted history and origin of the helicoids is suspected to be torsional, with the heliaxis coinciding with the torsion axis, as illustrated in Fig. 10, and explained below. The first deformation stage involved a modest rotation of +5° per kilometer along the gently-

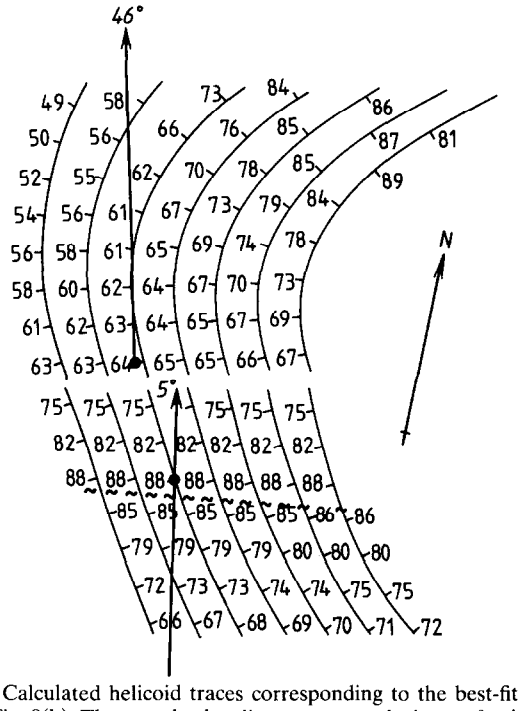

Fig. 9. Calculated helicoid traces corresponding to the best-fit pole loci in Fig. 8(b). The wavy broken line represents the locus of points of surface dip reversal.

plunging heliaxis, perhaps to accommodate the dilation produced by early stages of intrusion of the adjacent Davys Creek Granite. The northern modestly-rotated cleavage trends then suffered more intense torsion along a steeper heliaxis, perhaps coinciding with the development of the Vale Creek and Mt Evernden Faults, which are estimated to have accommodated a torsional rotation of between +8 and +9.5° per kilometer. This later episode of more intense torsion may have been required by the rapid inflation of the Davys Creek Granite in its final intrusive phase (Fowler 1994).

Some distortion of cleavage trend curvature is likely to have occurred due to flattening around the late syntectonic Davys Creek Granite. However, the modest

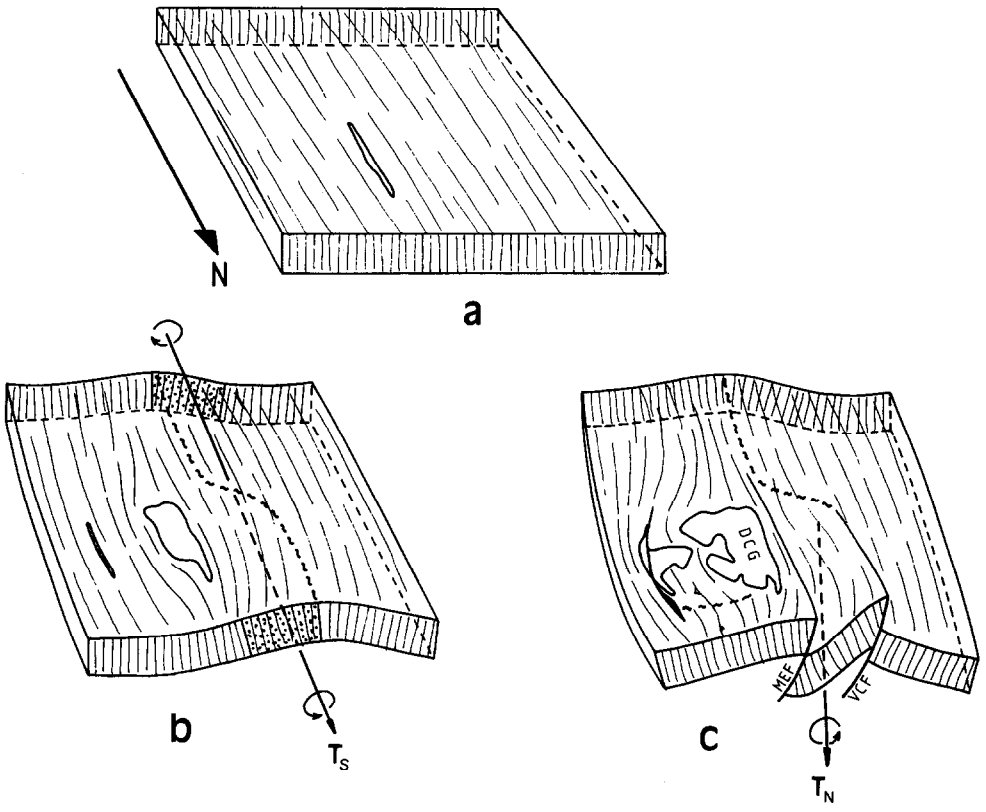

Fig. 10. Interpreted history of distortion of regional cleavages around the late syn-tectonic Davys Creek Granite (DCG). As with other figures, the locus of points of dip direction reversal is shown. Note that north points towards the observer. (a) Original steep to vertical cleavages across the region. Onset of intrusion of the Davys Creek Granite. (b) Modest torsion of cleavages about gently plunging T_s torsion axis. (c) Development of the Vale Creek Fault (VCF) and torsion about the northerly plunging T_N torsion axis. MEF = Mt Evernden Fault.

curvature of cleavage trends along the eastern side of the granite suggests that this effect may not be great. Stevens (1975) has questioned whether the strong curvature of cleavage trends in the northernmost part of the mapped area in Fig. 7 was due to emplacement of the Bathurst Granite. This is doubtful because (i) there are insignificant strain effects in the aureole of the Bathurst Granite associated with its intrusion (Paterson *et al.* 1991); (ii) the Mt Evernden Fault transects the curved cleavages and predates the Bathurst Granite (Fowler 1989); (iii) the cleavage trends elsewhere along the southern contact of the granite and those north of the Bathurst Granite are not deflected as they approach the contact; and (iv) satellite plutons of the Bathurst Granite show no deflection of cleavages at their margins (Packham 1968, Bateman 1982). The accommodation of torsion between two curviplanar faults is an example of the types of boundaries that may separate torsional from non-torsional domains. This is further discussed in the next section.

POSSIBLE ORIGINS OF HELICOIDS

Helicoids and helical lineations obviously may be generated by torsional forces. The possibilities of torsional deformation in structural geology have largely been ignored, possibly due to (i) the rejection of initially popular ideas of the role of torsion in jointing (Hills 1972, p. 105); (ii) the notion that planar surfaces suppress torsion because of the potentially large displacements at increasing distance from the torsion axis, and relating to this, (iii) problems attending the nature of boundaries separating torsional and non-torsional domains. Nevertheless, Billings (1972, p. 159) thought it probable that 'torsion is an important type of deformation', and Nevin (1949, p. 21) felt that 'torsional stresses are present far more frequently than is commonly suspected', and (Nevin, 1949, p. 136) 'during the warping of an area into a broad uplift, torsional stresses are bound to occur'. However, the principles formalised by Paterson & Weiss (1961) regarding the geometry of deformed objects, require only that the symmetry elements which are common to all factors of deformation (i.e. are present in both the undeformed object and in the deforming forces) are also present in the deformed object. There may be any number of additional symmetry elements in the deformed object which are not present in the deforming forces. Stated simply, torsional forces may produce helicoids, but are *not* a necessity.

Regional compression, horizontal shear and torsion about a vertical axis have been invoked by Tokuda (1926) and Lee (1929) to explain curviplanar en échelon fold belt structural trends in Eastern Asia. However, Hills (1972, p. 334) questioned whether basement

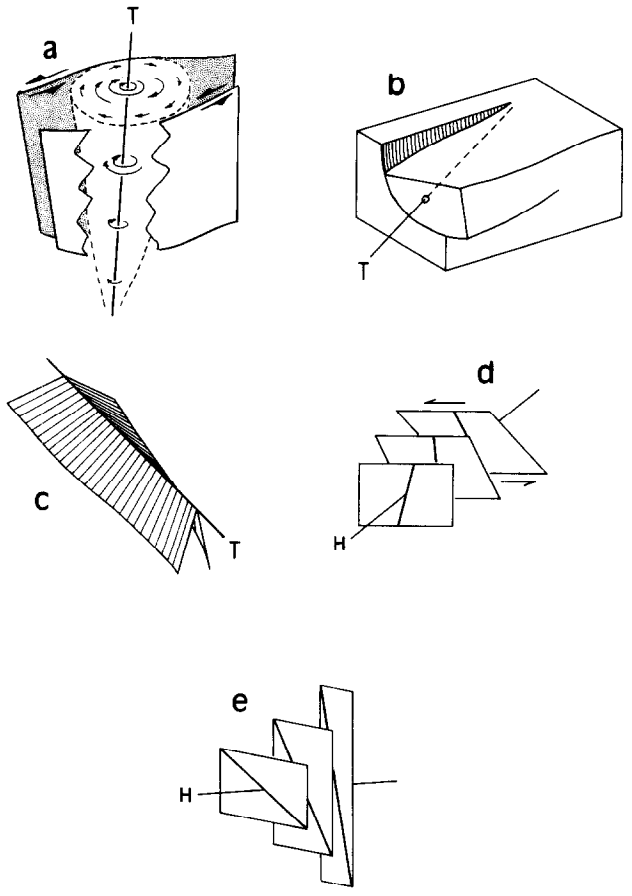

Fig. 11. (a) Torsion of a cylindrical volume bound by shears. (b) Torsion on a cylindrical scissor-fault. (c) The limbs of a chevron with decreasing interlimb angle follow the shape of a helicoid. (d) A helicoid surface could be traced only by passive progressive rotation of lines (e.g. bedding intersections on cleavage planes) in a rotational strain field. (e) Similar to (d) but in an irrotational strain field.

shearing beneath the cover may be responsible for these peculiar fold trends. de Sitter (1964, p. 159) referred to torsional motion (presumably in cover rocks) due to unequal vertical movements of the basement possibly being involved in the development of normal faults in cover rocks. Allerton (1994) described differential rotation of the upper limb of a recumbent fold clockwise with respect to the lower limb by several tens of degrees about a vertical axis, in response to differential shortening radially outwards from this axis.

The helical rise of magma in diapirs intruding active shear zones described by Hippertt (1994) is torsional in its dynamics. This provides an example of a boundary separating domains which have experienced torsion from those which have not. A sketch of such a boundary is shown in Fig. 11(a), where angular displacement decreases to zero at the intrusive contact where frictional resistance to flow reaches a maximum. The boundary surfaces may be ductile shear zones, in which case the angular displacement need not fall to zero at the domain boundary. The spiral cross-sections of rotational porphyroblasts (Fig. 2a) also show radial gradients in angular displacement.

A variation on the shear boundary model between torsional and non-torsional domains is shown in Fig. 11(b), where the boundary is curviplanar (the termination of a cylindrical, conical or listric fault). Similar boundaries are suggested to enclose the helicoidal domain of the southern Hill End Trough, described above. Listric thrust slices bound by converging thrust splays (i.e. horses) could experience a rotation gradient normal to the shear direction, leading to helicoidal geometry. Examples of regional cleavage fans being dissected by listric thrusts are shown by Weber (1981) and Weijermars (1986).

The simplest (and most likely) geological objects to show torsional strain will be linear or cylinder-shaped. In engineering, the problems of torsion of cylindrical shells (e.g. pipes) are routinely considered (Calladine 1983), and the hinges of tight folds may be approximations to cylindrical shells, at least near the hinges. Linear fabrics and anisotropies such as those described by Watkinson (1983) may also experience torsional strains.

Another example of torsion is shown in Fig. 11(c) where the torsion axis is a chevron fold hinge. A progressive change in interlimb angle along the hinge will generate a helicoid geometry in the fold limbs.

Whereas torsion involves the body rotation of radial segments of the deformed surface, the passive rotation of these segments in a rotational or irrotational strain field may also generate helicoids. Such helicoids are produced independently of torsion, as noted above. Two examples are shown in Figs. 11(d) & (e). A shear strain gradient (Fig. 11d, e.g. disposed laterally outwards from the centre of a ductile shear zone) would be expected to generate helicoid geometry in pre-existing inclined surfaces. An additional complexity is introduced by the likely curvature of the heliaxis (producing a non-regular helicoid) due to the gradient of X strain values accompanying the shear strain gradient, which at higher values is also responsible for development of sheath folds. In this example, the boundaries enclosing the torsional domain are those of the ductile shear zone itself.

A helicoid produced in an irrotational strain field is shown in Fig. 11(e). Again, curvature of the heliaxis is likely. Such a strain gradient might be expected as a zone of constriction is approached, e.g. near the triple points around syntectonic expanding plutons (Brun & Pons 1981, Guglielmo 1993), or near the stem of a rising diapir (Dixon 1975).

Acknowledgements—The author has benefited from earlier helpful comments by Vince Cronin and Ray Fletcher. The text of this paper was improved by constructive suggestions by Dan Schultz, Susan Treagus and an anonymous referee. I would like to thank Paul Lennox for his encouragement to pursue this topic.

REFERENCES

Allerton, S. 1994. Vertical-axis rotation associated with folding and thrusting: an example from the eastern Subbetic zone of southern Spain. *Geology*, **22**, 1039–1042.

Anderson, E. M., 1951. *The Dynamics of Faulting*. Oliver & Boyd, Edinburgh.

Bateman, R. 1982. The zoned Bruinbun granitoid pluton and its aureole. *J. geol. Soc. Aust.* **29**, 253–265.

Billings, M. P. 1972. *Structural Geology*, 3rd Edition. Prentice-Hall Inc., Englewood Cliffs, New Jersey.
Borowski, E. J. & Borwein, J. M. 1989. *Dictionary of Mathematics*. Harper Collins, London.
Bouchez, J. L., Gleizes, G., Djouadi, T. & Rochette, P. 1990. Microstructure and magnetic susceptibility applied to emplacement kinematics of granites: the example of the Foix pluton (French Pyrenees). *Tectonophysics* **184**, 157–171.
Brun, J. P. & Pons, J. 1981. Strain patterns of pluton emplacement in a crust undergoing non-coaxial deformation. *J. Struct. Geol.* **3**, 219–229.
Calladine, C. R. 1983. *Theory of Shell Structures*. Cambridge University Press, Cambridge.
Collins, A. G. 1971. The morphology of slaty cleavage in the Hill End Trough, NSW. Unpublished Ph.D Thesis, University of Sydney.
Delaney, P. T. & Pollard, D. D. 1981. Deformation of host rocks and flow of magma during growth of minette dikes and breccia-bearing intrusions near Ship Rock, New Mexico. *U.S. Geol. Survey Prof. Pap.* **1202**.
de Sitter, L. U. 1964. *Structural Geology*, 2nd Edition, McGraw-Hill, New York.
Dixon, J. M. 1975. Finite strain and progressive deformation in models of diapiric structures. *Tectonophysics* **28**, 89–124.
Fink, J. H. 1985. Geometry of silicic dikes beneath the Inyo Domes, California. *J. geophys. Res.* **90**, 11127–11133.
Fowler, T. J. 1987. A stratigraphic, structural and tectonic analysis of the Rockley District, New South Wales. Unpublished Ph.D. Thesis, University of Sydney.
Fowler, T. J. 1989. Superposed folding in the Rockley district, Lachlan Fold Belt, New South Wales. *Aust. J. Earth Sci.* **36**, 451–468.
Fowler, T. J. 1994. Sheeted and bulbous intrusion mechanisms of a small granitoid from southeastern Australia: implications for dyke-to-pluton transformation during emplacement. *Tectonophysics* **234**, 197–215.
Guglielmo, G. 1993. Interference between pluton expansion and non-coaxial tectonic deformation: three-dimensional computer model and field implications. *J. Struct. Geol.* **125**, 593–608.
Hills, E. S. 1972. *Elements of Structural Geology*, 2nd Edition. Wiley, New York.
Hippertt, J. F. 1994. Structures indicative of helicoidal flow in a migmatitic diapir (Bação Complex, southeastern Brazil). *Tectonophysics* **234**, 169–196.
James, R. C. & James, G. 1992. *Mathematics Dictionary*, 5th Edition. Van Nostrand Reinhold, New York.
Johnson, S. E. 1993. Unravelling the spirals: a serial thin-section study and three-dimensional computer-aided reconstruction of spiral-shaped inclusion trails in garnet porphyroblasts. *J. metam. Geol.* **11**, 621–634.
Lee, J. S. 1929. Some characteristic structural types in Eastern Asia and their bearing on the problem of continental movements. *Geol. Mag.* **66**, 358–522.
Lisle, R. J. 1992. Constant bed-length folding: three-dimensional geometrical implications. *J. Struct. Geol.* **14**, 245–252.
Mandl, G. 1987. Discontinuous fault zones. *J. Struct. Geol.* **9**, 105–110.
Nevin, S. M. 1949. *Principles of Structural Geology*, 3rd Edition. Wiley, New York.
O'Driscoll, E. S. T. 1980. The double helix in global tectonics. *Tectonophysics* **63**, 397–417.
Packham, G. H. 1968. Bathurst 1:250,000 Geological Sheet. Geological Survey of New South Wales, Sydney.
Paterson, M. S. & Weiss, L. E. 1961. Symmetry concepts in the structural analysis of deformed rocks. *Bull. geol. Soc. Am.* **72**, 841–882.
Paterson, S. R., Fowler, T. J., Vernon, R. H. & Flood, R. H. 1991. Contrasting styles and timing of emplacement of Murrumbidgee- and Bathurst-type batholiths in the Lachlan Fold Belt, Australia. *Geol. Soc. Aust. Abs.* **29**, 42.
Powell, C. McA. 1984. Uluru and Adelaidean regimes. In: *Phanerozoic Earth History of Australia* (edited by Veevers, J. J.). Clarendon Press, Oxford, 270–350.
Powell, D. & Treagus, J. E. 1967. On the geometry of *S*-shaped inclusion trails in garnet porphyroblasts. *Mineralog. Mag.* **36**, 453–456.
Powell, D. & Treagus, J. E. 1970. Rotational fabrics in metamorphic minerals. *Mineralog. Mag.* **37**, 801–814.
Ramsay, J. G. 1967. *Folding and Fracturing of Rocks*. McGraw-Hill, New York.
Rosenfeld, J. L. 1970. Rotated garnets in metamorphic rocks. *Spec. Pap. geol. Soc. Am.* **129**.
Schoneveld, C. 1977. A study of some typical inclusion patterns in strongly paracrystalline rotated garnets. *Tectonophysics* **39**, 453–471.
Stanton, R. L. 1956. The Palaeozoic rocks of the Wiseman's Creek — Burraga area, NSW. *J. & Proc. Roy. Soc. N.S.W.* **89**, 131–156.
Stauffer, M. R. 1964. The geometry of conical folds. *N.Z. Jl Geol. Geophys.* **7**, 340–347.
Stevens, B. P. 1975. A metallogenic study of the Bathurst 1:250,000 Sheet. Geological Survey of New South Wales, Sydney.
Tokuda, S. 1926. On the échelon structure of the Japanese Archipelagoes. *Jap. J. Geol. Geog.* **5**, 41–76.
Turner, F. J. & Weiss, L. 1963. *Structural Analysis of Metamorphic Tectonites*. McGraw-Hill, New York.
Watkinson, A. J. 1981. Patterns of fold interference: influence of early fold shape. *J. Struct. Geol.* **3**, 19–23.
Watkinson, A. J. 1983. Patterns of folding and strain influenced by linearly anisotropic bands. *J. Struct. Geol.* **5**, 449–454.
Weber, K. 1981. The structural development of the Rheinische Schiefergebirge. *Geol. Mijnb.* **60**, 149–159.
Weijermars, R. 1986. S_1-cleavage fans in the Moselmulde of the Rheinische Schiefergebirge (Federal Republic of Germany) may be due to a D_3-tectonic event: open folding and reverse faulting. *Geol. Rdsch.* **75**, 323–332.
Weiss, L. E. & McIntyre, D. B. 1957. Structural geometry of Dalradian rocks at Loch Leven, Scottish Highlands. *J. Geol.* **65**, 575–602.
Wilson, G. 1967. The geometry of cylindrical and conical folds. *Proc. geol. Assoc. London* **78**, 179–210.

APPENDIX

Derivation of equations for the general helicoid

First, consider a three-axis coordinate system with z as the heliaxis. Before rotation, a set of initially parallel planar surfaces may be represented by the equation:

$$\mathbf{h}x + \mathbf{k}y + \mathbf{l}z - d = 0. \tag{1}$$

where all of the planes have the same vector normal ($\mathbf{h}, \mathbf{k}, \mathbf{l}$), and the planes differ in their d values.

To generate the helicoid surface, every point (x,y,z) on each plane experiences a rotational transformation to (x',y',z'). The amount of rotation is a function of the z-component, most simply linearly related to z via the constant θ. The transformation of coordinates is treated as a matrix operation:

$$\begin{bmatrix} x' \\ y' \\ z' \end{bmatrix} = \begin{bmatrix} \cos(\theta z) & \sin(\theta z) & 0 \\ -\sin(\theta z) & \cos(\theta z) & 0 \\ 0 & 0 & 1 \end{bmatrix} \begin{bmatrix} x \\ y \\ z \end{bmatrix}$$

which gives:

$$\begin{aligned} x' &= x\cos(\theta z) + y\sin(\theta z) \\ y' &= y\cos(\theta z) - x\sin(\theta z) \\ z' &= z. \end{aligned} \tag{2}$$

Substituting the transformed coordinates of equations (2) into (1) gives us the general equation for the helicoid:

$$\begin{aligned} f(x,y,z) = x[\mathbf{h}\cos(\theta z) - \mathbf{k}\sin(\theta z)] \\ + y[\mathbf{h}\sin(\theta z) + \mathbf{k}\cos(\theta z)] + \mathbf{l}z - d = 0. \end{aligned} \tag{3}$$

The vector coordinates for the pole to the surface at any (x, y, z) may be obtained with the gradient operator:

$$\nabla f = \left(\frac{\partial f}{\partial x}, \frac{\partial f}{\partial y}, \frac{\partial f}{\partial z}\right). \tag{4}$$

This gives the coordinates of the pole to the helicoid at (x, y, z):

$$\begin{aligned} \nabla f = (\mathbf{h}\cos(\theta z) - \mathbf{k}\sin(\theta z), \mathbf{h}\sin(\theta z) \\ + \mathbf{k}\cos(\theta z), \mathbf{l} + \theta(y\mathbf{h} - \mathbf{k}x)\cos(\theta z) \\ - \theta(y\mathbf{k} + \mathbf{h}x)\sin(\theta z)). \end{aligned} \tag{5}$$

Calculation of helicoid traces (curvilinear lines of intersection of a helicoid with a horizontal erosion surface)

For Figs. 4 & 5, where the heliaxis is buried but parallel to the erosion surface, the z- and y-axes are set horizontal, and x vertical. The

horizontal erosion surface then corresponds to the plane x = constant. This value for x is substituted into equation (3) to generate the equations for the level curves on the erosion surface. The pole coordinates for points along the level curves are also simply calculated again by substituting the desired value of x into equation (5). These pole coordinates are simply translated into trend and plunge of the pole, and from this into dips and strikes of the outcropping level curves at any point.

When the heliaxis is plunging, a new coordinate system is devised parallel and perpendicular to the ground surface (x_{new}, y_{new} and z_{new} axes). The z_{new}-axis is set along the trend of the plunging heliaxis with the origin of the new axes coinciding with the origin of the original axes, and therefore lying at the point of emergence of the heliaxis. Thus we need only deal with level curves for $x_{new} = 0$. f referred to the original axes may be related to the new axes by a matrix, which after multiplication gives:

$$\begin{aligned} x &= x_{new}\cos(\sigma) + z_{new}\sin(\sigma) \\ y &= y_{new} \\ z &= z_{new}\cos(\sigma) - x_{new}\sin(\sigma) \end{aligned} \tag{6}$$

where σ is the plunge of the heliaxis from the horizontal. Substituting (6) in (3), setting $x_{new} = 0$ and using the new axes as our x, y, z coordinate system, gives the equation for a helicoid with axis oblique to z:

$$\begin{aligned} g(x,y,z) = {} & z\sin(\sigma\{\mathbf{h}\cos(\psi) - \mathbf{k}\sin(\psi)\}) \\ & + y\{\mathbf{h}\sin(\psi) + \mathbf{k}\cos(\psi)\} + \mathbf{l}z\cos(\sigma) - d = 0 \end{aligned} \tag{7}$$

where $\psi = \theta z\cos(\sigma)$.

Again using the gradient operator, the coordinates for the poles to this helicoid at point $(0, y, z)$ are:

$$\begin{aligned} \nabla g = {} & (P\{\cos(\sigma) - y\theta\sin(\sigma)\} + Q\theta z\sin^2(\sigma) \\ & - \mathbf{l}\sin(\sigma),\ Q,\ P\{\sin(\sigma) + y\theta\cos(\sigma)\} \\ & - Q\theta z\sin(\sigma)\cos(\sigma) + \mathbf{l}\cos(\sigma)) \end{aligned} \tag{8}$$

where

$$P = \mathbf{h}\cos(\psi) - \mathbf{k}\sin(\psi)$$

$$Q = \mathbf{h}\sin(\psi) + \mathbf{k}\cos(\psi).$$

The common pole on stereograms

When $P = 0$, i.e. when $z = \{\tan^{-1}(\mathbf{h}/\mathbf{k})\}/\theta\cos(\sigma)$, the $\nabla\mathbf{g}$ vector coordinates depend only on z. Therefore, along the line $z = \{\tan^{-1}(\mathbf{h}/\mathbf{k})\}/\theta\cos(\sigma)$, all the outcropping helicoid surfaces have the same pole (the common pole). The vector coordinates for this common pole are:

$$\begin{aligned} \Delta\mathbf{g}_{common} = {} & (\sin(\sigma)\tan(\sigma)\{\tan^{-1}(\mathbf{h}/\mathbf{k})\}\sqrt{(\mathbf{h}^2 + \mathbf{k}^2)} \\ & - \mathbf{l}\sin(\sigma),\ \sqrt{(\mathbf{h}^2 + \mathbf{k}^2)},\ \mathbf{l}\cos(\sigma) \\ & - \sin(\sigma)\{\tan^{-1}(\mathbf{h}/\mathbf{k})\}\sqrt{(\mathbf{h}^2 + \mathbf{k}^2)}). \end{aligned} \tag{9}$$

Similar arguments lead to the vector coordinates for the common pole in the case of non-plunging heliaxis, though in this case we must take account of x since the erosion surface is not necessarily the plane $x = 0$. The common pole vector coordinates become:

$$\nabla f_{common} = (0,\ \sqrt{(\mathbf{h}^2 + \mathbf{k}^2)},\ \mathbf{l} - \theta x\sqrt{(\mathbf{h}^2 + \mathbf{k}^2)}). \tag{10}$$

The zero first vector coordinate indicates that the common pole always represents a vertical plane.